Science of the Total Environment 651 (2019) 2772–2786

Contents lists available at ScienceDirect

Science of the Total Environment

journal homepage: www.elsevier.com/locate/scitotenv

Climate change will constrain the rapid urban expansion in drylands: A scenario analysis with the zoned Land Use Scenario Dynamics-urban model

Zhifeng Liu [a,b], Yanjie Yang [a,b], Chunyang He [a,b,*], Mengzhao Tu [a,b]

[a] Center for Human-Environment System Sustainability (CHESS), State Key Laboratory of Earth Surface Processes and Resource Ecology (ESPRE), Faculty of Geographical Science, Beijing Normal University, Beijing 100875, China
[b] School of Natural Resources, Faculty of Geographical Science, Beijing Normal University, Beijing 100875, China

HIGHLIGHTS

- The impacts of climate change on urban expansion in APTZNC in 2015–2050 are evaluated.
- The climate change would be a key factor affecting the urban expansion in this region.
- The urban land affected by climate change would rise by 5–12 folds.
- The impacts would be the most significant in the mid-western sub-region of APTZNC.
- The zoned LUSD-urban model can more effectively simulate the urban expansion.

GRAPHICAL ABSTRACT

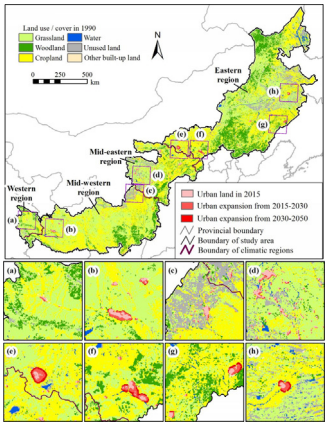

ARTICLE INFO

Article history:
Received 28 August 2018
Received in revised form 12 October 2018
Accepted 12 October 2018
Available online 13 October 2018

Editor: Deyi Hou

Keywords:
Drylands
Urban expansion
Climate change
Systems dynamics model
Cellular automata model

ABSTRACT

Evaluation of climate change impacts (CCIs) on urban expansion is important to improving the urban sustainability in drylands. Taking the agro-pastoral transitional zone of northern China (APTZNC) as an example, this study evaluates potential CCIs on urban expansion in 2015–2050. First, we set up six climate change scenarios (CCSs) based on the simulated results of global climate model and regional climate model under different representative concentration pathways. Then, we simulate regional urban expansion under the different CCSs using the zoned Land Use Scenario Dynamics-urban (LUSD-urban) model. We find that climate change will be a key factor that affects urban expansion in this region. The urban land affected by climate change in the entire region will increase from 20.24–26.48 km^2 (2020) to 119.71–339.26 km^2 (2050), an increase of 4.91–11.81 times. The CCIs on urban expansion will be the most significant in the mid-western region. In 2050, the urban land potentially affected by climate change will be 98.70–213.88 km^2, which is 42.26%–134.12% of the urban land in the entire region. To improve urban sustainability in the APTZNC, effective measures must be adopted to mitigate and adapt to CCIs on urban expansion.

* Corresponding author at: State Key Laboratory of Earth Surface Processes and Resource Ecology, Beijing Normal University, 19 Xinjiekouwai Street, Beijing 100875, China.
E-mail address: hcy@bnu.edu.cn (C. He).

https://doi.org/10.1016/j.scitotenv.2018.10.177
0048-9697/

1. Introduction

Drylands are regions that experience a lack of water resources that restrict primary production and nutrient cycling (MEA, 2005). The increasing problems of poverty, ecosystem services degradation and climate change sensitivity in drylands are affecting global sustainable development (Reynolds et al., 2007; UNDP-DDC, 2007, 2014). Recently, mainly driven by extensive socioeconomic development, the urban land has expanded rapidly in drylands, which is (UN, 2014; Z. Liu et al., 2016, 2017). The rapid urban expansion in drylands worldwide is causing a series of ecological and environmental problems (e.g., biodiversity decline, cropland loss, water shortages and environmental pollution), which in turn affect the sustainability of such regions (UNDP-DDC, 2014; J. Li et al., 2016, 2017; He et al., 2017). In addition, the rapid urban expansion in drylands is facing severe challenges from climate change (IPCC, 2013). In drylands such as northern and southern Africa, western Asia, northern America and western Australia, average temperatures in summer and winter in 2016–2035 will increase by approximately 1 °C. In addition, multi-year average precipitation and runoff will decrease by 10%, a decrease that could reach 30% in certain local areas (IPCC, 2013). Clearly, climate change will influence water availability and thus affect the urban expansion in drylands (Magadza, 2000; S. Li et al., 2017). Analysis of climate change impacts (CCIs) on urban expansion can support urban planning, and is important for urban sustainability in drylands (Magadza, 2000; Deng et al., 2013; Wu, 2013, 2014).

Previous studies have evaluated the CCIs on urban expansion in drylands at various scales. At the regional scale, Huang et al. (2014) examined the CCIs on urban expansion in 13 provinces in northern China in 2005–2030 and found that regional urban expansion will continue. At the local scale, He et al. (2015) investigated the CCIs on urban expansion in the Beijing-Tianjin-Tangshan region, and concluded that the regional urban land area will increase rapidly under climate change in 2009–2030. In contrast, Liu et al. (2018) projected that climate change will decrease the urban land area of China's Guanzhong area in 2010–2050. While such studies are helpful for understanding the CCIs on urban expansion in drylands, they exhibit defects in the selection of climate change scenarios (CCSs) and the simulation of urban expansion, causing significant uncertainties in their future projections. For example, Huang et al. (2014) set the future annual precipitation change rate at 0, 5%, and 10% and the future annual temperature increase at 0.5 °C, 1 °C, and 2 °C, subsequently subjectively selecting three from the nine possible combinations of the temperature trends and the precipitation trends to set the CCSs. This approach neglects the interactions among different factors (e.g., temperature and precipitation) in the climate system and makes it difficult to effectively predict future climate change characteristics. Additionally, the spatial heterogeneity of CCIs on urban expansion has not been considered in the simulation of urban expansion under climate change, thus resulting in errors in the projected results (Huang et al., 2014). Therefore, exiting studies do not effectively reflect CCIs on urban expansion in drylands.

Representative concentration pathways (RCPs) provide reliable CCSs for studying CCIs on urban expansion in drylands. The RCPs represent the next generation of greenhouse gas change pathways developed by the Intergovernmental Panel on Climate Change (IPCC) in 2009 (Moss et al., 2010; IPCC, 2013, 2014). The RCPs include four pathways (i.e., RCP2.6, RCP4.5, RCP6.0 and RCP8.5) which represent four representative greenhouse gas emission pathways that adopt different climate mitigation and adaptation strategies (van Vuuren et al., 2011). Compared to previous greenhouse gas emission pathways, the RCPs can better reflect the effects of climate mitigation and adaptation strategies, providing a reliable way to characterize future CCSs (Moss et al., 2010). At present, the RCPs have been successfully used to simulate urban expansion under climate change. For example, X. Li et al. (2016) projected global urban expansion in 2010–2100 using the RCPs. Similarly, Jiang et al. (2014) modeled urban expansion in China's Pearl River Delta region in 2005–2030 based on the RCPs.

The Land Use Scenario Dynamics-urban (LUSD-urban) model represents a reliable method to simulate CCIs on urban expansion. It is a regional urban expansion simulation model developed by coupling the system dynamics (SD) model and the cellular automata (CA) model (He et al., 2005, 2008, 2017). It can be used to effectively simulate urban expansion under CCSs by integrating macroscopic and microcosmic factors that influence urban expansion (He et al., 2015). Based on this model, urban expansion under climate change in 13 provinces in northern China in 2005–2030 and the in Beijing-Tianjin-Tangshan region in 2009–2030 have been simulated (Huang et al., 2014; He et al., 2015). However, the LUSD-urban model does not consider the spatial heterogeneity of climate change and urban expansion. These limitations hinder its ability to simulate large-scale urban expansion with reasonable accuracy (He et al., 2015). The zoned LUSD-urban model overcomes the limitations of the former model through first dividing an entire region into several sub-regions according to the natural and socioeconomic characteristics of the region and then simulating the urban expansion in each sub-region. Compared with the single LUSD-urban model, the zoned LUSD-urban model can effectively characterize the spatial heterogeneity of regional climate change and urban expansion and more accurately simulate urban expansion under CCIs. However, few studies have been performed using the zoned LUSD-urban model.

This study aims to quantitatively assess and understand the CCIs on urban expansion in drylands by using the agro-pastoral transitional zone of northern China (APTZNC) as a case study area. We first set up the CCSs, and then use the zoned LUSD-urban model to simulate urban expansion in the APTZNC in 2015–2050 under climate change. We evaluate the CCIs on regional urban expansion by contrasting the simulation results obtained in different CCSs. The study results offer support for improving urban sustainability in drylands.

2. Study area and data

2.1. Study area

The APTZNC is an ecotone between the agricultural area and the pastoral area in northern China. It is a semi-arid region with mean annual precipitation of 250–500 mm (Wang et al., 1999; Shi et al., 2009). The region is facing problems such as water resources shortage, environmental deterioration and climate change sensitivity. Rapid socio-economic development is accelerating urban expansion in the region. Therefore, the region is suited for studying urban expansion in drylands under climate change (Hao et al., 2017).

The study region is located between 100°E–125°E and 34°N–49°N, with an area of 0.73 million km^2, representing 8.11% of the Chinese territory (Fig. 1). It is located in a transitional area, with a climate that changes from a sub-humid continental monsoon climate to a drought-prone typical continental climate. The mean annual temperature is 2–8 °C. The region's elevation increases progressively from northeast to southwest, whereby the lowest and highest elevations are 200 m and 4500 m, respectively (Wang et al., 1999; Shi et al., 2009). Its major soil types are calcareous soil, chestnut soil, chernozem and aeolian sandy soil. Its natural landscapes are characterized by a transition from forest grassland to shrub grassland to desert steppe, while the landscapes modified by human activities exhibit a transition from agricultural land to pastureland.

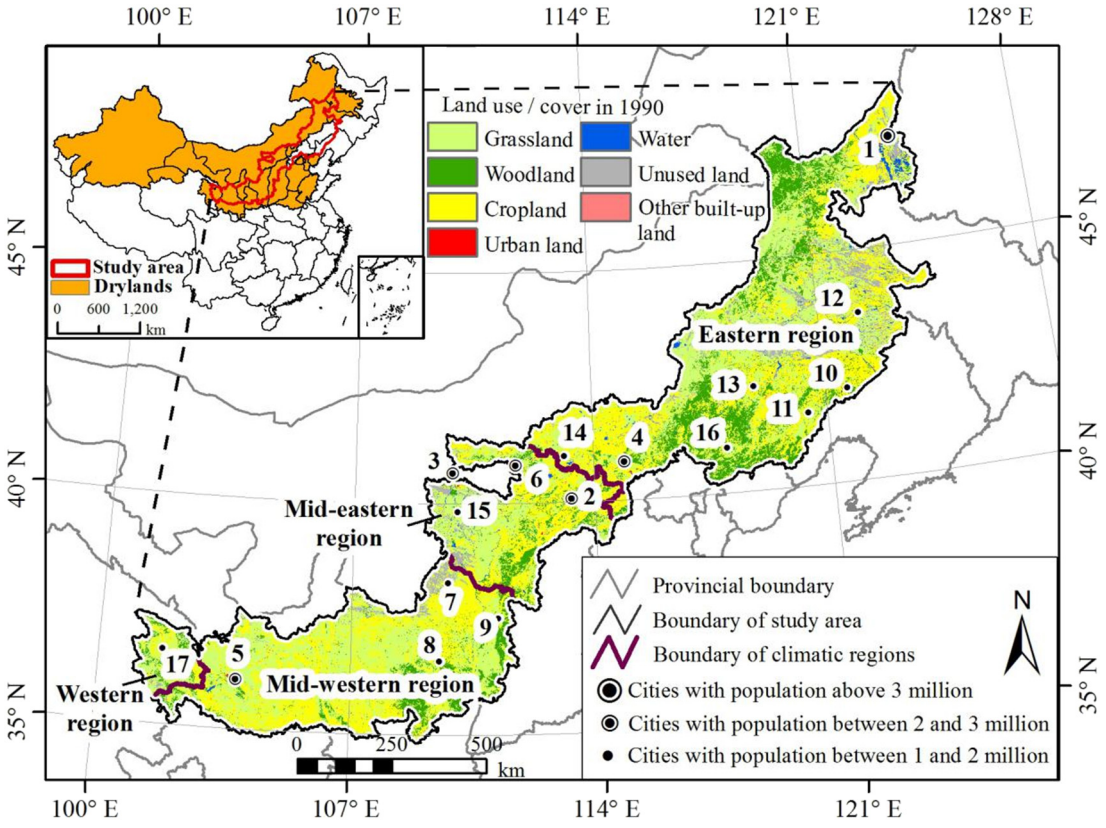

Fig. 1. The study area. *The cities with population above 1 million were listed in the figure, which include Qiqihar (1), Datong (2), Baotou (3), Zhangjiakou (4), Lanzhou (5), Hohhot (6), Yulin (7), Yan'an (8), Lvliang (9), Fuxin (10), Chaoyang (11), Tongliao (12), Chifeng (13), Ulanqab (14), Ordos (15), Chengde (16), Xining (17).

The APTZNC encompasses 39 cities and 10 provinces including Inner Mongolia, Shanxi and Shaanxi. In 2010, the total population was 66.81 million. The urban population was 29.65 million and the urbanization rate was 44.38% (NBSC, 2016). Among the region's 39 cities, Qiqihar numbers over 3 million inhabitants, and five cities, including Lanzhou, Zhangjiakou and Hohhot, have populations of 2–3 million. Additionally, 11 cities, including Yulin, Ordos and Xining, number 1–2 million inhabitants (Fig. 1).

2.2. Data

The urban land data for 1992–2015 with a spatial resolution of 1 km were obtained from the urban land information dataset in China, which was established by He et al. (2014) and Xu et al. (2016). The data have been validated as having high accuracy (average overall accuracy: 92.62%; quantity error: 1.49%; position error: 5.89%; Kappa coefficient: 0.60).

The land use/cover data for 1990 with a spatial resolution of 1 km were obtained from the National Land Use/Cover Datasets (http://www.geodata.cn/Portal/index.jsp). These datasets were established based on imagery, such as Landsat TM/ETM+ and HJ-1/1B, and have an overall classification accuracy over 90% (Liu et al., 2014).

The meteorological observation data were derived from the meteorological science data sharing service network (http://data.cma.cn). We extracted the mean annual temperature and precipitation data for each site in the study area for 2000–2015. On this basis, the mean annual temperature and precipitation with a spatial resolution of 1 km were prepared through the spatial interpolation of the site data using the kriging interpolation method (Pei et al., 2013).

The climate simulation data (covering the average annual temperature and precipitation) for 2006–2050 are based on the outputs of global climate model (GCM) and regional climate model (RCM) under RCP2.6, RCP4.5 and RCP8.5. We use the outputs of seven GCMs in this study: BNU-ESM, CanESM2, CCSM4, IPSL-CM5A-LR, MPI-ESM-LR, MRI-CGCM3 and NorESM1-M (Table S1). These models were downloaded from the World Climate Research Programme (WCRP) CMIP5 Climatic Mode Dataset, released by the Program for Climate Model Diagnosis and Intercomparison (PCMDI) (https://esgf-node.llnl.gov/search/cmip5). Following Egan and Mullin (2016), the ensemble mean annual temperature and precipitation of the seven GCMs are used to represent the overall GCM outputs. The RCM data used in this study are long-term climate change data simulated by the China National Climate Center using a regional climate model (RegCM4.0) (China regional climate change prediction data network: http://www.climatechange-data.cn/en/; Table S1).

The socio-economic statistical data for 2000–2015 included the urban population and gross regional product (GDP) obtained from the provincial statistical yearbook and the water resources quantity and water consumption quantity obtained from the provincial water resources bulletin. The digital elevation model (DEM) data were downloaded from the Geospatial Data Cloud Platform of Computer Network Information Center, Chinese Academy of Sciences (http://www.gscloud.cn). The basic geographic information data (including the administrative boundaries, administrative centers, national roads, provincial roads, highways and railways in the APTZNC) were sourced from the National Geomatics Center of China (http://ngcc.sbsm.gov.cn).

3. Methods

3.1. Setting the future climate change scenarios (CCSs)

Following the IPCC Fifth Assessment Report, we set the future CCSs based on RCP2.6, RCP4.5 and RCP8.5 (Fig. 2) (IPCC, 2014). Among these

future CCSs, RCP2.6 is characterized by radiative forcing that peaks in 2010–2020 and declines thereafter. Its radiative forcing in 2100 is 2.6 W/m^2 above that of preindustrial levels. Based on RCP2.6, the global temperature will increase by 1 °C in 2006–2100 (IPCC, 2014). RCP2.6 represents a world with very strict emission reduction policies. Thus, it predicts the least greenhouse gas emission and the smallest temperature increase of the RCPs. In contrast, RCP4.5 is characterized by radiative forcing that peaks near 2040 and stabilizes thereafter at 4.5 W/m^2 above preindustrial levels. RCP4.5 assumes a world with a moderate emission reduction policy, in which the global temperature will increase by 1.8 °C in 2006–2100 (IPCC, 2014). RCP8.5 represents a greenhouse gas emission pathway with radiative forcing steadily increasing beyond the 21st century. Its radiative forcing in 2100 reaches 8.5 W/m^2 above preindustrial levels. The global temperature is expected to increase by 3.7 °C in 2006–2100 under this pathway (IPCC, 2014). Compared to the other RCPs, RCP8.5 has the highest greenhouse gas emission and temperature increase because it reflects a world in which no emission reduction measures are adopted.

A climate model is a set of mathematical equations that characterize climate system dynamics following physical and chemical laws. The use of such models has become the mainstream approach for simulating climate change under different scenarios (IPCC, 2014). Based on the simulation scale, the climate models can be classified as GCM and RCM (Giorgi et al., 2012; IPCC, 2014). A GCM can comprehensively reflect the global climate change process, whereas a RCM can effectively describe regional climate characteristics. To account for the uncertainty of the simulation results of these climate models, both GCM and RCM simulation results were adopted under future CCSs. On this basis, we set up six CCSs (including GCM-RCP2.6, GCM-RCP4.5, GCM-RCP8.5, RCM-RCP2.6, RCM-RCP4.5 and RCM-RCP8.5) for use in this study (Table 1).

3.2. The zoned LUSD-urban model

Given the distinctive nature of climate change characteristics in different regions (He et al., 2015), the zoned LUSD-urban model is adopted to simulate urban expansion in the APTZNC

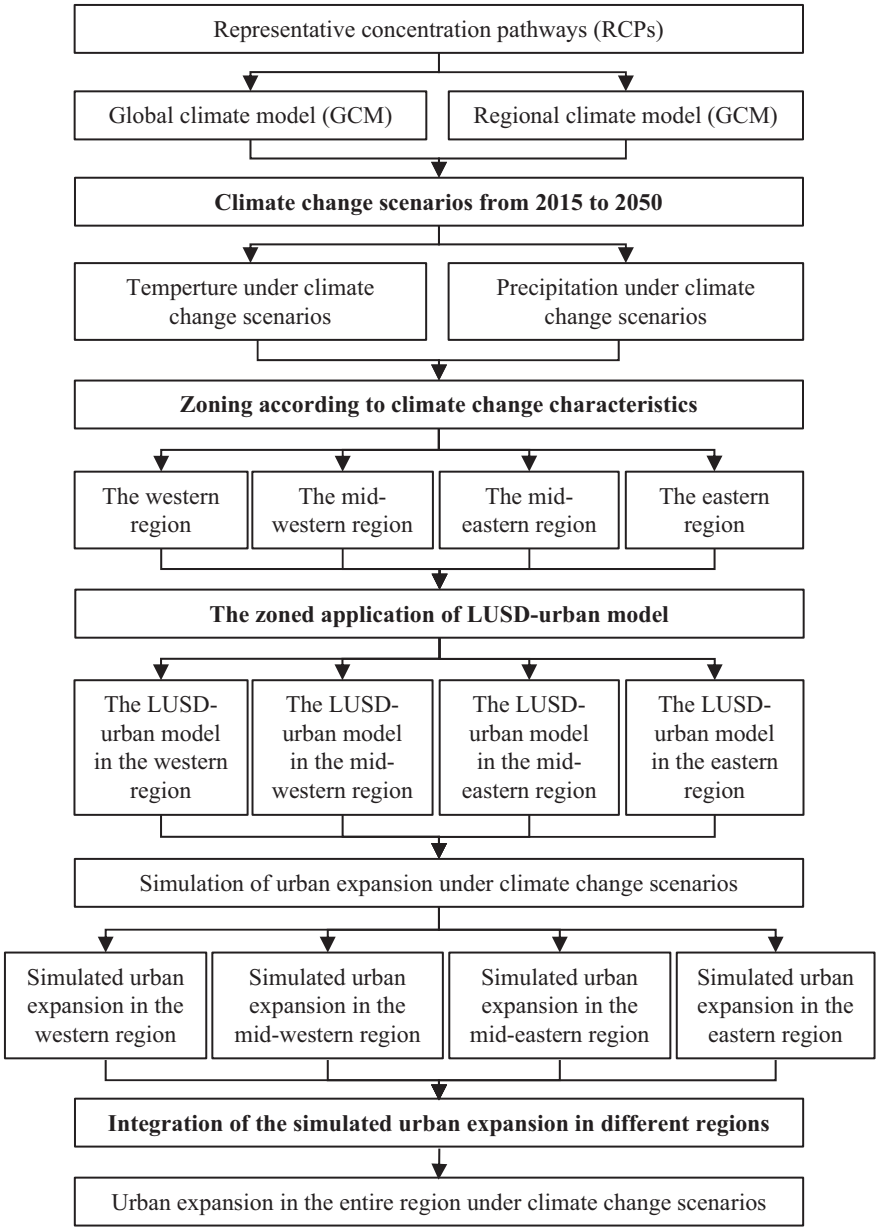

Fig. 2. The flow chart.

Table 1
The scenarios of climate change.

Climate model	Scenario	Climatic region	Change in mean annual temperature from 2015 to 2050 (°C)[a]	Change in annual precipitation from 2015 to 2050[a]
GCM	RCP2.6	Western	0.81	7.04%
		Mid-western	0.98	2.26%
		Mid-eastern	1.12	4.29%
		Eastern	1.09	8.46%
	RCP4.5	Western	1.26	6.04%
		Mid-western	1.37	4.83%
		Mid-eastern	1.37	13.04%
		Eastern	1.30	15.49%
	RCP8.5	Western	1.75	13.77%
		Mid-western	1.72	13.46%
		Mid-eastern	1.68	10.22%
		Eastern	1.82	10.91%
RCM	RCP2.6	Western	0.98	−11.77%
		Mid-western	0.70	2.67%
		Mid-eastern	0.74	−3.61%
		Eastern	0.70	2.59%
	RCP4.5	Western	0.91	14.57%
		Mid-western	1.16	5.09%
		Mid-eastern	1.02	18.41%
		Eastern	0.98	18.37%
	RCP8.5	Western	1.82	22.75%
		Mid-western	1.68	9.04%
		Mid-eastern	1.51	13.27%
		Eastern	1.61	10.22%

[a] The change in mean annual temperature and the change in annual precipitation were calculated using the linear trend analysis according to Shi et al. (2014).

under climate change (Fig. 2). First, the entire research region is divided into several sub-regions according to regional climate change characteristics. Then, in each sub-region, the LUSD-urban model is applied to simulate urban expansion under different CCSs. For each CCS, the simulation results for the sub-regions are integrated to calculate the urban expansion for the entire region.

3.2.1. Zoning based on climate change characteristics

Based on the climate change characteristics of the APTZNC in 1961–2010 (Shi et al., 2014), the region is divided into four sub-regions: western, mid-western, mid-eastern and eastern (Fig. 1). The climate change characteristics of these sub-regions differ significantly in 2006–2050 (Table 1). In the western region, the average annual temperature will increase 0.81–1.82 °C, and the annual precipitation change rate will be between 11.77% and 22.75%. The average annual temperature in the mid-western region will increase 0.70–1.72 °C, and annual precipitation will increase 2.26%–13.46%. In the mid-eastern region, the average annual temperature will increase 0.74–1.68 °C, and the annual precipitation change rate will be approximately 3.61%–18.41%. The average annual temperature in the eastern region will increase 0.70–1.82 °C, and annual precipitation will increase 2.59%–18.37% (Table 1).

3.2.2. Simulation of urban expansion based on zoned LUSD-urban model

The LUSD-urban model combines an urban land demand simulation module based on the SD model and an urban land spatial allocation module based on the CA model. Basically, it first simulates regional urban land demand, and then generates the spatial distribution of regional urban land according to the principle of balance between urban land supply and demand (He et al., 2008, 2015). In consideration of the characteristics of drylands, we used water resources as the limiting factor to represent the CCIs on urban expansion (Schimel, 2010; McDonald et al., 2011; Pravalie, 2016). First, we assumed that climate change would alter urban land demand through its impact on regional water resources (He et al., 2015). Based on this assumption, the urban land demand simulation modules of the LUSD-urban model in four sub-regions were constructed to simulate the urban land demand under climate change (Fig. 3). Based on the regional urban population carrying capacity and the economic carrying capacity constrained by water resources (Cohen, 1995; Long et al., 2004; Xie et al., 2005), this module first simulates the regional urban population and GDP. Then, it uses these intermediate outputs to estimate the regional urban land demand (Fig. 3). The maximum urban population carrying capacity constrained by water resources is expressed as follows:

$$UPCC_i = \frac{w_i \varepsilon_i WR_i}{WC_i} \quad (1)$$

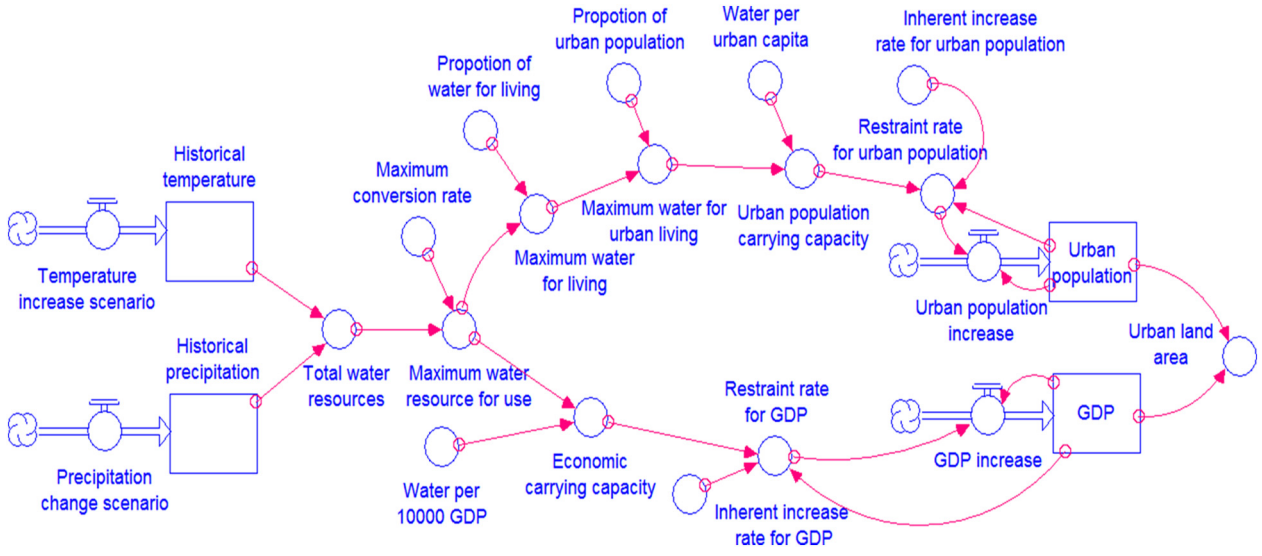

Fig. 3. The structure of the SD-based urban land demand module in the LUSD-urban model.

where $UPCC_i$ is the maximum urban population carrying capacity in the *ith* sub-region, WR_i is the amount of water resources in the *ith* sub-region, WC_i is the water consumption per capita in the *ith* sub-region, and w_i and ε_i are the proportion of urban water consumption to water resources and the water supply capacity factor in the *ith* sub-region, respectively. The maximum economic carrying capacity constrained by water resources is estimated as follows:

$$ECC_i = \frac{\varepsilon_i WR_i}{WC_{GDP,i}} \tag{2}$$

where ECC_i is the maximum economic carrying capacity in the *ith* sub-region, and $WC_{GDP,i}$ is the amount of water consumption per unit GDP in the region. The regional water resources can be calculated as follows:

$$WR_i = a_i P_i + b_i T_i + c_i \tag{3}$$

where P_i and T_i are the mean annual precipitation and temperature in the *ith* sub-region, and a_i, b_i and c_i are regression coefficients.

Following He et al. (2005, 2015), we hypothesize that the spatial allocation of urban land is primarily influenced by suitability, inheritance and neighborhood. Based on this assumption, the spatial allocation of urban land is simulated using LUSD-urban models for the four sub-regions. Specifically, we calculate the probability of all non-urban pixels being converted to urban pixels in the sub-regions. The calculation is given by the following:

$${}^tP_{K,i,j} = \left(\sum_{n=1}^{m-2} W_n \cdot {}^tS_{n,i,j} + W_{m-1} \cdot {}^tN_{i,j} - W_m \cdot {}^tI_{K,i,j}\right) \cdot \prod_{r=1} {}^tEC_{r,i,j} \cdot \prod_{l=1} {}^tPC_{l,i,j} \cdot {}^tV_{i,j} \tag{4}$$

where ${}^tP_{K,i,j}$ is the probability of the *jth* non-urban pixel with K land cover type in the *ith* sub-region being converted to a urban pixel at *t* time, ${}^tS_{n,i,j}$ is

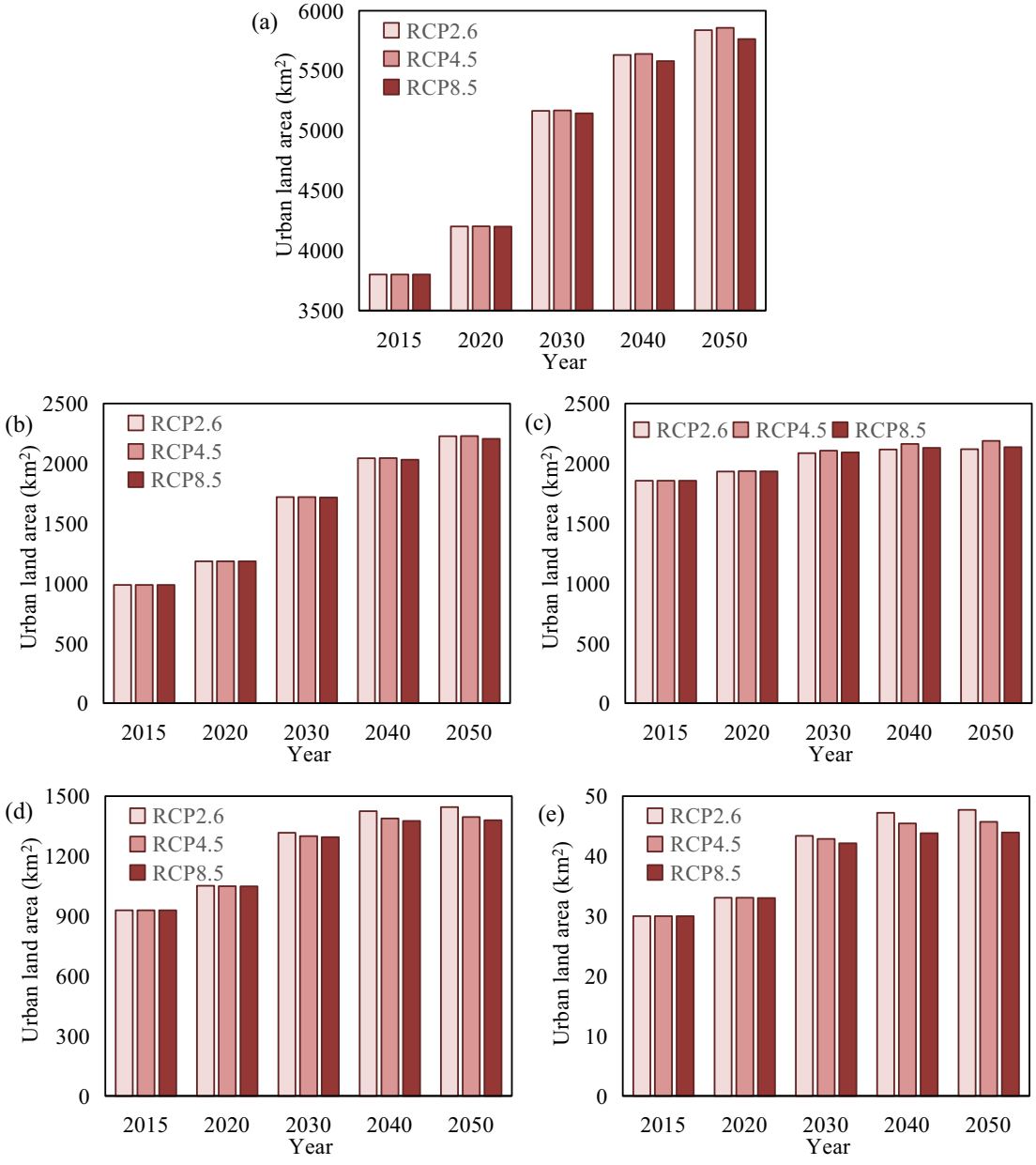

Fig. 4. The urban expansion under CCSs based on GCM. (a) The urban expansion in the APTZNC; (b) the urban expansion in the eastern region; (c) the urban expansion in the mid-eastern region; (d) the urban expansion in the mid-western region; (e) the urban expansion in the western region.

the standardized value of the *nth* suitability factor, W_n is the weight of the suitability, ${}^tN_{i,j}$ is the neighboring effect of the pixel, W_{m-1} is the weight of the neighboring effect, ${}^tI_{K,i,j}$ is the influence of inheritance, W_m is the weight of the inheritance impact, ${}^tEC_{r,i,j}$ denotes the ecological limitations, ${}^tPC_{l,i,j}$ indicates the limitations of land planning and land use policies, and ${}^tV_{i,j}$ indicates random interference factors. ${}^tV_{i,j}$ is calculated as follows:

$$ {}^tV_{i,j} = 1 + [-\ln(rand)]^a \quad (5) $$

where *rand* is a random variable with a uniform distribution ranging between 0 and 1, and *a* is an adjustment factor for controlling the random disturbances degree. In each sub-region, one year is adopted as a simulation cycle. The no-urban pixels with the highest probability of being converted to urban pixels are selected first in a simulation cycle, and these selected pixels are converted to urban pixels. We repeat this conversion process until the total amount of urban land matches the urban land demand under climate change.

3.2.3. Integration of simulation results

After simulating the urban expansion in each sub-region, we integrate the simulation results to obtain the urban expansion

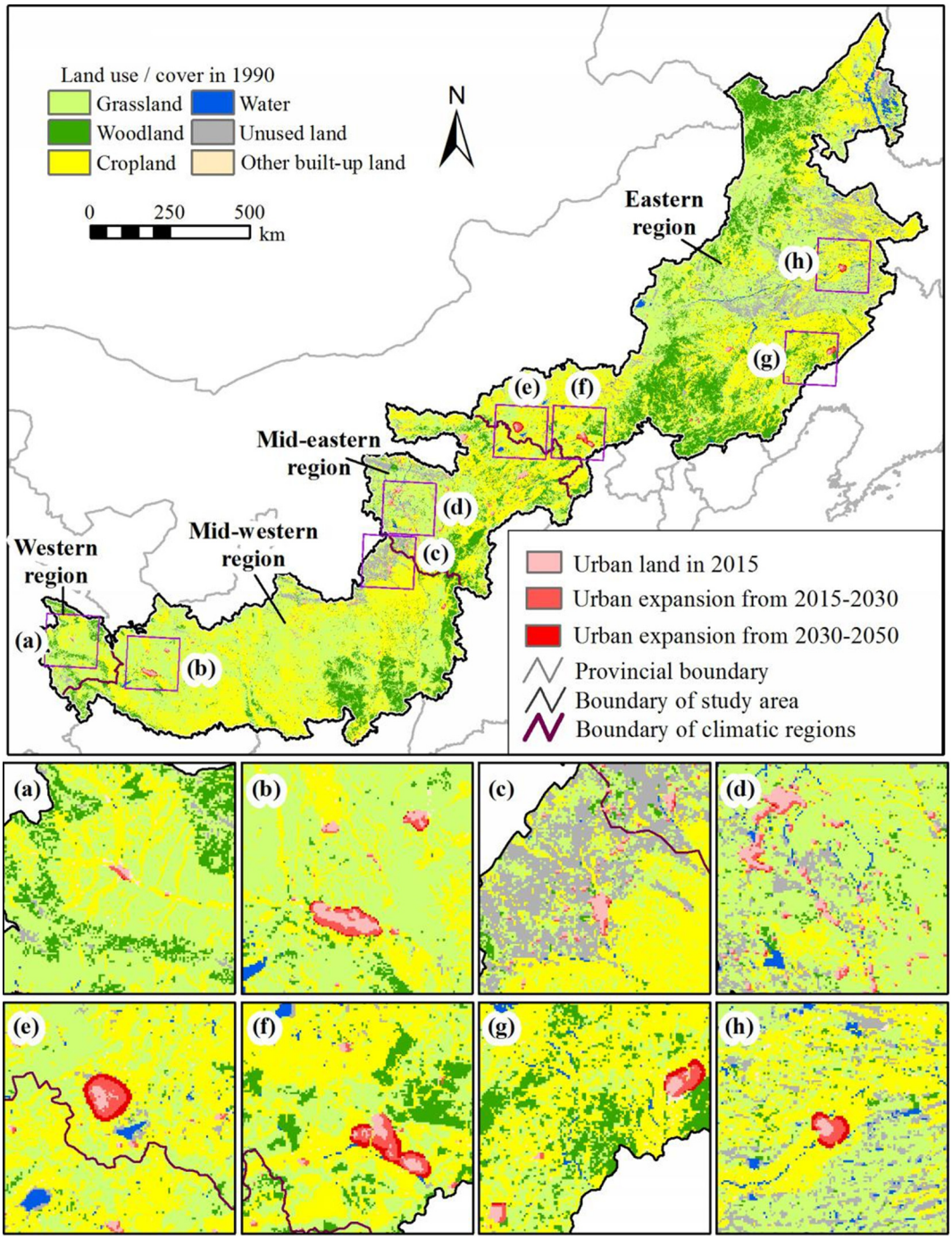

Fig. 5. The spatial patterns of urban expansion under GCM-RCP4.5. *The eight cities with the largest urban expansion area were listed including Xining (a), Lanzhou (b), Yulin (c), Ordos (d), Ulanqab (e), Zhangjiakou (f), Fuxin (g), and Tongliao (h).

information for the entire region. The integration process is expressed as follows:

$$ {}^{t}UL_j = \begin{cases} {}^{t}UL_j^{Western} & if\left(R_j^{Western}=1\right) \\ {}^{t}UL_j^{Mid-western} & if\left(R_j^{Mid-western}=1\right) \\ {}^{t}UL_j^{Mid-eastern} & if\left(R_j^{Mid-eastern}=1\right) \\ {}^{t}UL_j^{Eastern} & if\left(R_j^{Eastern}=1\right) \end{cases} \quad (6) $$

where ${}^{t}UL_j$ indicates whether the *jth* image element is urban land at *t* time, and $R^{Western}{}_j$, $R^{Mid\text{-}western}{}_j$, $R^{Mid\text{-}eastern}{}_j$ and $R^{Eastern}{}_j$ denote whether the pixel belonged to the western, mid-western, mid-eastern or the eastern sub-region, respectively ('1' means 'yes', '0' means 'no'). ${}^{t}UL^{Western}{}_j$, ${}^{t}UL^{Mid\text{-}western}{}_j$, ${}^{t}UL^{Mid\text{-}eastern}{}_j$ and ${}^{t}UL^{Eastern}{}_j$ indicate whether a pixel in the attributive region is an urban pixel or otherwise.

3.3. Simulation of urban expansion under climate change

Following He et al. (2015), we calibrate the urban land demand simulation module of the LUSD-urban model using the temperature, precipitation, water resources, urban population, GDP and urban land data for each sub-region in 2000–2015. Similar to Shen et al. (2009) and Verburg et al. (2013), we perform sensitivity analysis and accuracy evaluation on the calibrated module. The sensitivity analysis reveals that the sensitivity factors to urban population are 0.32 and 0.44; and the sensitivity factors to GDP are 0.23 and 0.29 (Table S2). The accuracy evaluation reveals that the relative errors of urban population, GDP and urban land area are 2.28%, 0.96% and 4.34%, respectively. The absolute values of all relative errors are less than 5% (Table S3). These results indicate that the LUSD-urban model has high stability and reliability, and could effectively simulate urban land demand.

Based on the regional urban expansion data for 1992–1995, we use the Monte Carlo method to calibrate the urban land spatial allocation module of the LUSD-urban model for each sub-region. The simulation cell size was 1 km × 1 km, while the simulation period was one year. Water bodies identified in the land use/cover data were regarded as restricted areas for urban expansion according to He et al. (2015). The factors for elevation; slope; distances to provincial capitals, city centers and county centers; and distances to highways, national roads, provincial roads, and railways were used for calculating land suitability (Table S4). To evaluate the accuracy of the calibrated modules, we calculated the Kappa coefficients of the urban land simulation results for the APTZNC. The Kappa coefficients in 2000, 2010 and 2015 were 0.75, 0.64 and 0.65 respectively, suggesting that the LUSD-urban model could accurately simulate the spatial allocation of urban land.

These satisfactory validations give us the confidence to adopt the calibrated model to project the urban expansion in the APTZNC under six future CCSs. Based on these GCM-RCPs and RCM-RCPs, we analyze the urban expansion (of the entire region, sub-regions and major cities) in 2015–2050.

4. Results

4.1. Future urban expansion under GCM

Based on the GCM-RCPs, the urban land area in the APTZNC will steadily expand with an annual growth rate of 1.20–1.24% in 2015–2050 (Figs. 4 and 5, Table 2). The urban land area in the entire

Table 2
The change of urban land area under CCSs.

Climate model	Scenario	Climatic region	Urban land area (km^2)					Annual change rate from 2015 to 2050
			2015	2020	2030	2040	2050	
GCM	RCP2.6	Western	30	33	43	47	48	1.33%
		Mid-western	929	1052	1317	1425	1446	1.27%
		Mid-eastern	1855	1933	2085	2116	2118	0.38%
		Eastern	986	1184	1719	2043	2226	2.35%
		The entire region	3800	4201	5164	5631	5837	1.23%
	RCP4.5	Western	30	33	43	45	46	1.21%
		Mid-western	929	1049	1300	1388	1395	1.17%
		Mid-eastern	1855	1935	2106	2162	2188	0.47%
		Eastern	986	1184	1719	2044	2228	2.36%
		The entire region	3800	4201	5169	5640	5857	1.24%
	RCP8.5	Western	30	33	42	44	44	1.10%
		Mid-western	929	1049	1295	1376	1380	1.14%
		Mid-eastern	1855	1933	2091	2129	2136	0.40%
		Eastern	986	1184	1716	2031	2205	2.33%
		The entire region	3800	4199	5144	5580	5764	1.20%
RCM	RCP2.6	Western	30	33	43	46	46	1.24%
		Mid-western	929	1051	1324	1447	1486	1.35%
		Mid-eastern	1855	1932	2080	2106	2106	0.36%
		Eastern	986	1184	1720	2046	2232	2.36%
		The entire region	3800	4200	5167	5645	5870	1.25%
	RCP4.5	Western	30	33	43	47	48	1.34%
		Mid-western	929	1050	1309	1409	1424	1.23%
		Mid-eastern	1855	1938	2130	2214	2269	0.58%
		Eastern	986	1184	1722	2052	2243	2.38%
		The entire region	3800	4205	5204	5722	5984	1.31%
	RCP8.5	Western	30	33	42	44	44	1.11%
		Mid-western	929	1049	1292	1368	1371	1.12%
		Mid-eastern	1855	1935	2104	2158	2180	0.46%
		Eastern	986	1184	1717	2034	2211	2.33%
		The entire region	3800	4200	5155	5604	5806	1.22%

region is projected to increase from 3800 km^2 to 5764–5857 km^2 (Fig. 4a, Table 2). In the GCM-RCP4.5 scenario, the urban land area of the entire region will increase most rapidly, with an annual growth rate of 1.24% (Fig. 4a, Table 2). In the GCM-RCP8.5 scenario, the urban land area in the entire region will expand at a slightly slower rate of 1.20% (Fig. 4a, Table 2).

The future urban expansion appears to proceed unevenly among the sub-regions (Figs. 4 and 5, Table 2). The urban land in the eastern region will increase most rapidly. The urban land in this region will increase at an annual growth rate of 2.33–2.36%, a rise from 986 km^2 (2015) to 2205–2228 km^2 (2050) (Fig. 4b, Table 2). In contrast, the urban expansion rate in the mid-eastern region is the slowest (0.38–0.47%), where its urban land area is projected to increase from 1855 km^2 (2015) to 2118–2188 km^2 (2050) (Fig. 4c, Table 2).

Among the major cities, the urban expansion in Fuxin, Tongliao, Tongchuan and Zhangjiakou in 2015–2050 will be significantly higher than in other cities (Fig. 5). The Fuxin city will experience the fastest urban expansion rate (3.91%), with the urban land area increasing from 64 km^2 (2015) to 245 km^2 (2050). During the same period, the urban land area of Tongliao, Tongchuan and Zhangjiakou will expand at an annual growth rate of over 3%, while that of other cities will be slower (less than 2%).

4.2. Future urban expansion under RCM

Based on the RCM-RCPs, the urban land area in the APTZNC will increase significantly over the projection period (Figs. 6 and 7, Table 2). In 2015–2050, the urban land area in the entire region will increase from 3800 km^2 to 5806–5984 km^2, with an annual growth rate of 1.22–1.31% (Fig. 6a, Table 2). The urban expansion rate of the APTZNC is the fastest (slowest) in the RCM-RCP4.5 (RCM-RCP8.5) with an average annual growth rate of 1.31% (1.22%) (Fig. 6a, Table 2).

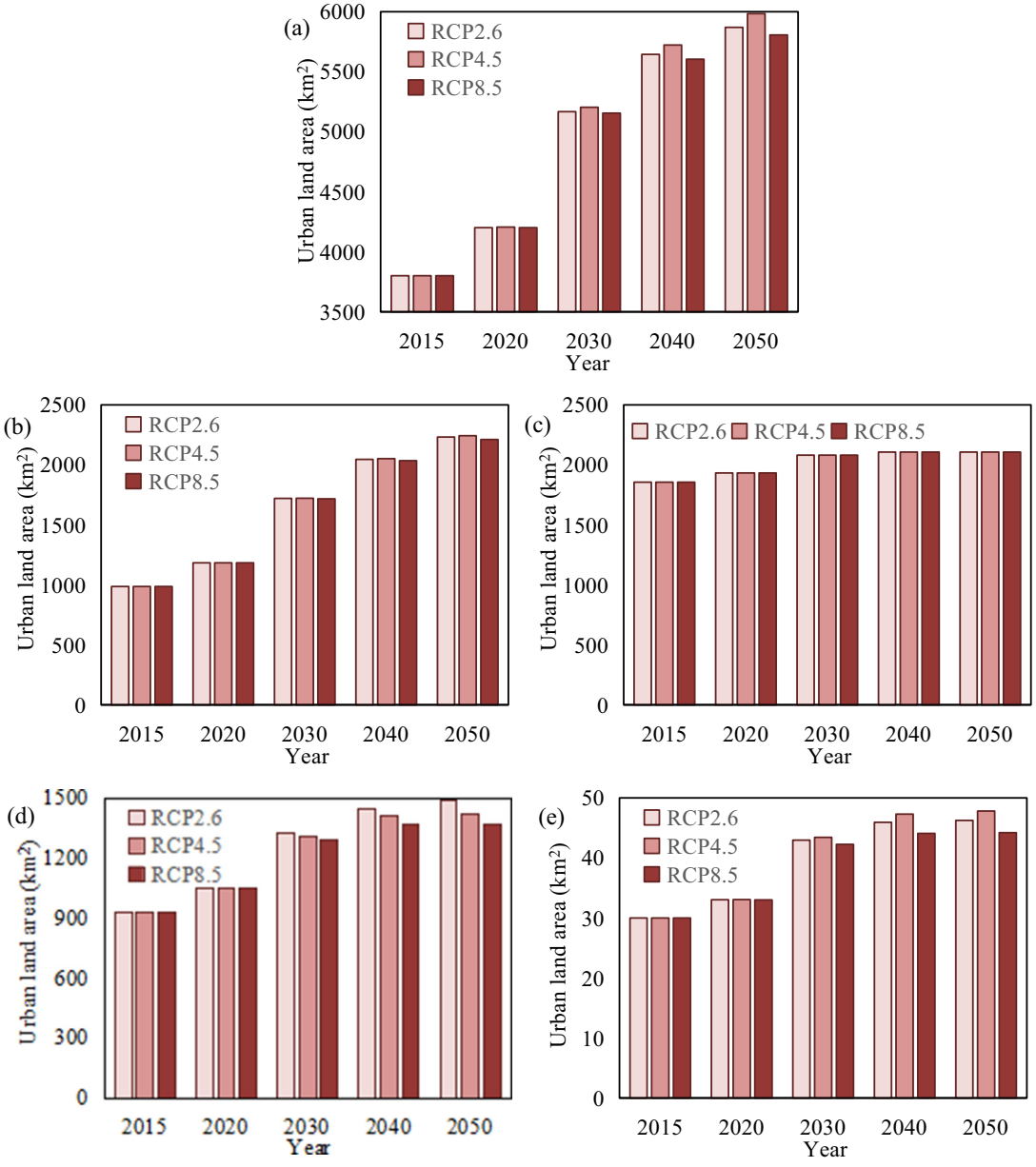

Fig. 6. The urban expansion under CCSs based on RCM. (a) The urban expansion in the APTZNC; (b) the urban expansion in the eastern region; (c) the urban expansion in the mid-eastern region; (d) the urban expansion in the mid-western region; (e) the urban expansion in the western region.

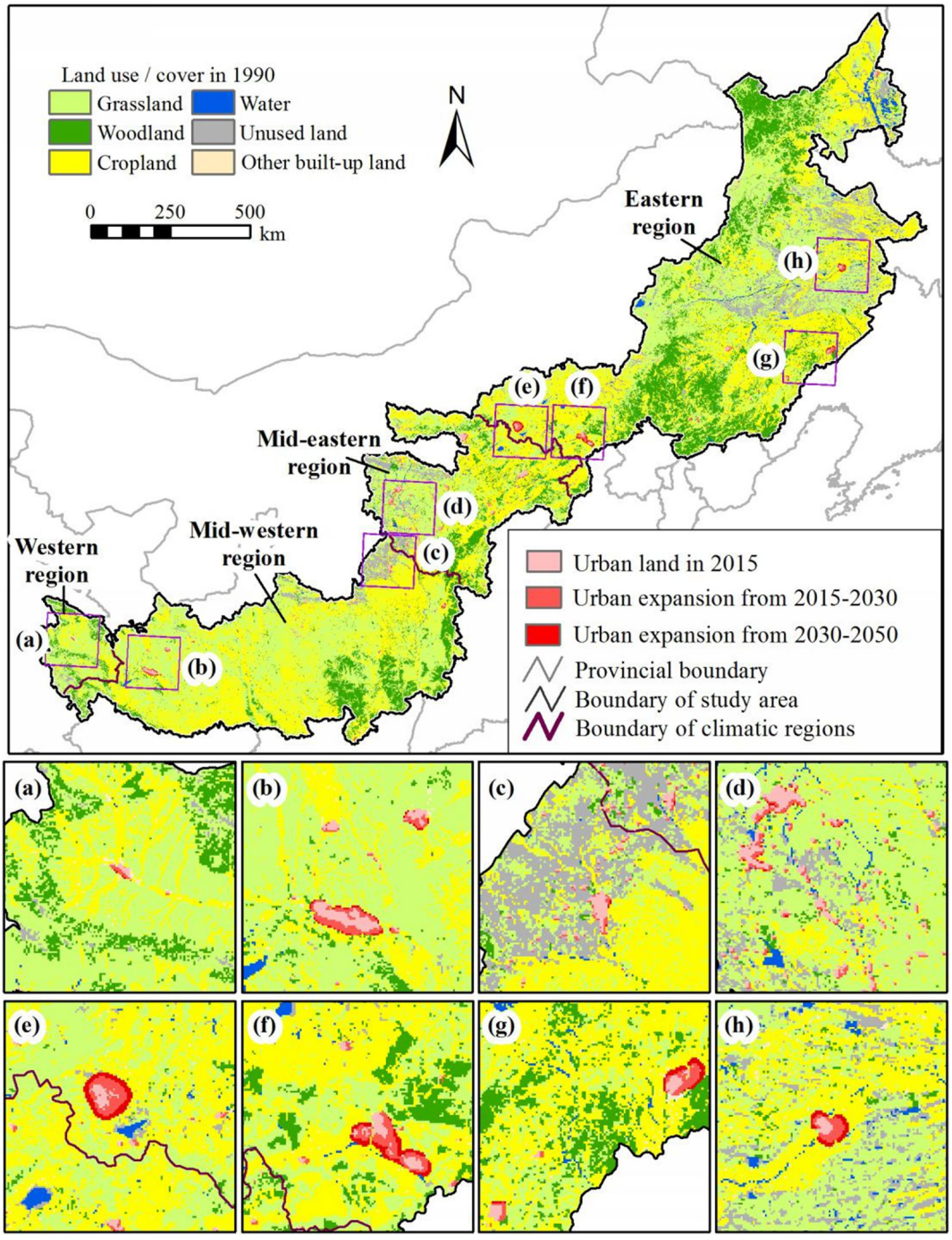

Fig. 7. The spatial patterns of urban expansion under RCM-RCP4.5. *The eight cities with the largest urban expansion area were listed including Xining (a), Lanzhou (b), Yulin (c), Ordos (d), Ulanqab (e), Zhangjiakou (f), Fuxin (g), and Tongliao (h).

The urban expansion in the eastern region will be faster than in other regions (Figs. 6 and 7, Table 2). The urban land area in the eastern region will expand at an annual rate of 2.33–2.38%, i.e., increase from 986 km^2 to 2211–2243 km^2 in 2015–2050 (Fig. 6b, Table 2). In contrast, the urban expansion in the mid-eastern region will be the slowest (i.e., an annual increase of 0.36–0.58%). There, the urban land area is projected to increase from 1855 km^2 to 2106–2269 km^2 in 2015–2050 (Fig. 6c, Table 2). Comparatively, the urban expansion rate in the eastern region will be 4–7 times that in the mid-eastern regions.

The annual growth rates of urban area in Fuxin, Tongliao, Tongchuan, Zhangjiakou and Ulanqab will be significantly higher than in other cities (Fig. 7). Among these five cities, the annual urban area growth rate in Fuxin will be the highest (3.91–3.96%), followed by Tongliao and Tongchuan (3.5%), and then Zhangjiakou and Ulanqab (approximately 3%). The average annual urban land area growth rates in other cities will be less than 2%.

5. Discussions

5.1. The zoned LUSD-urban model can more effectively simulate the CCIs on urban expansion

First, the zoned LUSD-urban model comprehensively considered regional differences among the CCIs and the influences of socio-economic development on urban expansion, and could

Table 3
The comparison of accuracy of simulated urban land area between the single LUSD-urban model and the zoned LUSD-urban model.

	Relative error of simulated urban population in different years			Relative error of simulated GDP in different years			Relative error of simulated urban land area in different years		
	2005	2010	2015	2005	2010	2015	2005	2010	2015
Single LUSD-urban model	5.72%	7.82%	10.63%	8.66%	3.48%	20.24%	15.00%	28.54%	11.90%
Zoned LUSD-urban model	2.74%	2.00%	2.28%	2.47%	8.31%	0.96%	16.71%	20.69%	4.33%
Difference between two models	−2.98%	−5.82%	−8.34%	−6.19%	4.82%	−19.28%	1.70%	−7.85%	−7.58%

improve the simulation precision of urban land demand. Following Shen et al. (2009), we evaluated the accuracy of the single LUSD-urban model and the zoned LUSD-urban model by analyzing the relative errors of urban population, GDP and land area simulation results in 2005, 2010 and 2015 (Table 3). We found that the relative error of the urban population based on the single LUSD-urban model is between 5.72% and 10.63%. The relative error of the simulated GDP is between 3.48% and 20.24%, and the relative error of the simulated urban land area is between 11.9% and 28.54% (Table 3). In contrast, the relative error of urban population simulated using the zoned LUSD-urban model is between 2% and 2.74%. The relative error of GDP is between 0.96% and 8.31%, and the relative error of urban land area is between 4.33% and 20.69% (Table 3). Comparatively, the relative errors of the zoned LUSD-urban model decreased by 2.98%–8.34%, 6.19%–19.28% and 7.58%–7.85% in terms of the simulated urban population, GDP and urban land area, respectively (Table 3).

Second, the zoned LUSD-urban model could reflect the differences in urban land suitability, inheritance and neighboring effect between different regions and could more accurately simulate the spatial allocation of urban land. Following He et al. (2008, 2015), we calculated the overall accuracy and Kappa coefficients for urban land in 2000, 2010 and 2015. We compared the accuracy of the simulation results of the single LUSD-urban model and the zoned LUSD-urban model (Table 4, Fig. 8). The overall accuracy for urban land simulated by the single LUSD-urban model ranges from 99.62%–99.92%, and the Kappa coefficient ranges from 0.59–0.72 (Table 4, Fig. 8). The overall accuracy of the urban land simulated by the LUSD-urban model ranges from 99.63%–99.95%, and the Kappa coefficient ranges from 0.64–0.75 (Table 4, Fig. 8). Comparatively, the overall accuracy of urban land simulation using the zoned LUSD-urban model increased by 0.01%–0.03%, and the Kappa coefficient increased by 1.56%–8.47% (Table 4, Fig. 8).

These outcomes indicate that the zoned LUSD-urban model could more effectively simulate urban expansion in the APTZNC under climate change. This model has the advantage of considering the natural and socio-economic conditions and the urban expansion characteristics of different regions (Shi et al., 2014; Liu et al., 2016; X. Liu et al., 2017). Therefore, it is suited for simulating urban expansion at different scales.

Table 4
The comparison of accuracy of simulated urban land patterns between the single LUSD-urban model and the zoned LUSD-urban model.

	Kappa coefficients in different years			Overall accuracy in different years		
	2000	2010	2015	2000	2010	2015
Single LUSD-urban model	0.72	0.59	0.64	99.92%	99.74%	99.62%
Zoned LUSD-urban model	0.75	0.64	0.65	99.95%	99.77%	99.63%
Difference between two models	4.17%	8.47%	1.56%	0.03%	0.03%	0.01%

5.2. The urban expansion rate will vary under different RCPs in the APTZNC

Under both GCM and RCM, the urban land area in the APTZNC will display different growth rates under the three RCPs (Table 2). The urban expansion rate will be the fastest for RCP 4.5 with average annual growth rates of 1.24% under GCM and 1.31% under RCM, followed by RCP2.6 with average annual growth rates of 1.23% under GCM and 1.25% under RCM between 2015 and 2050. In the same period, the urban expansion rate will be the lowest for RCP 8.5 with average annual growth rates of 1.20% under GCM and 1.22% under RCM. The average annual growth rates for RCP 4.5 will be 0.04% (0.09%) greater than for RCP 8.5 under GCM (RCM) in the APTZNC.

Among the sub-regions, the western region will exhibit the largest differences in urban expansion rate among the three RCPs (Table 2). Under GCM, the western region will have the highest average annual growth rate of 1.33% for RCP2.6 and the lowest average annual growth rate of 1.10% for RCP8.5, a difference of 0.23%. Under RCM, the western region will experience the fastest urban expansion, with an average annual growth rate of 1.34% for RCP4.5, and the slowest urban expansion, with an average annual growth rate of 1.11% for RCP8.5, a difference of 0.23%.

The different urban expansion rates are primarily caused by the different temperature and precipitation trends under the three RCPs (Table 1). In the western region, which exhibits the largest differences in urban expansion rate, the change in mean annual temperature from 2015 to 2050 for RCP8.5 (1.75 °C under GCM, 1.82 °C under RCM) will be approximately twice that for RCP 2.6 (0.81 °C under GCM, 0.98 °C under RCM). The change rate in annual precipitation from 2015 to 2050 for RCP8.5 (13.77% under GCM, 22.75% under RCM) will be 6%–33% larger than for RCP2.6 (7.04% for GCM, −11.77% under RCM). The different temperature and precipitation trends will result in varying water resources and further alter the urban land demand and urban expansion rate.

5.3. Climate change will affect urban sustainability in the APTZNC

Following He et al. (2015), we further evaluate the potential CCIs on the urban expansion in the APTZNC. Specifically, according to the temperature and precipitation conditions in 2015, we simulate the urban expansion of the APTZNC in 2015–2050 under a "no-climate-change-effect (NCCE)" scenario (Fig. S5). On this basis, we quantify the urban land area (of the entire region and the sub-regions) potentially affected by climate change by contrasting the differences between urban expansion under different CCSs and urban expansion under the NCCE scenario (Table 5, Fig. 9).

For the entire region, we find that the potential CCIs on regional urban expansion in the 2015–2050 will enhance. Under the GCM-RCPs, the area of urban land potentially affected by climate change in the entire region will increase from 23.97–26.48 km^2 (2020) to 246.04–339.26 km^2 (2050), an increase of 9.26–11.81 times (Table 5, Fig. 9a). The proportion of urban land area affected by climate change to the urban land area under NCCE will increase from 0.57%–0.63%

(2020) to 4.03%–5.56% (2050), an increase of 6.11–7.87 times (Fig. S5a). Based on the RCM-RCPs, the area of urban land potentially affected by climate change in the entire region will increase from 20.24–25.17 km^2 (2020) to 119.71–297.54 km^2 (2050), an increase of 4.91–10.86 times (Table 5, Fig. 9b). The proportion of urban land area affected by climate change to the urban land area under NCCE will increase from 0.48%–0.6% (2020) to 1.96%–4.88% (2050), an increase of 3.09–7.21 times (Fig. S5a).

Among the sub-regions, the urban expansion in the mid-western region will be influenced by climate change to an obvious extent. By

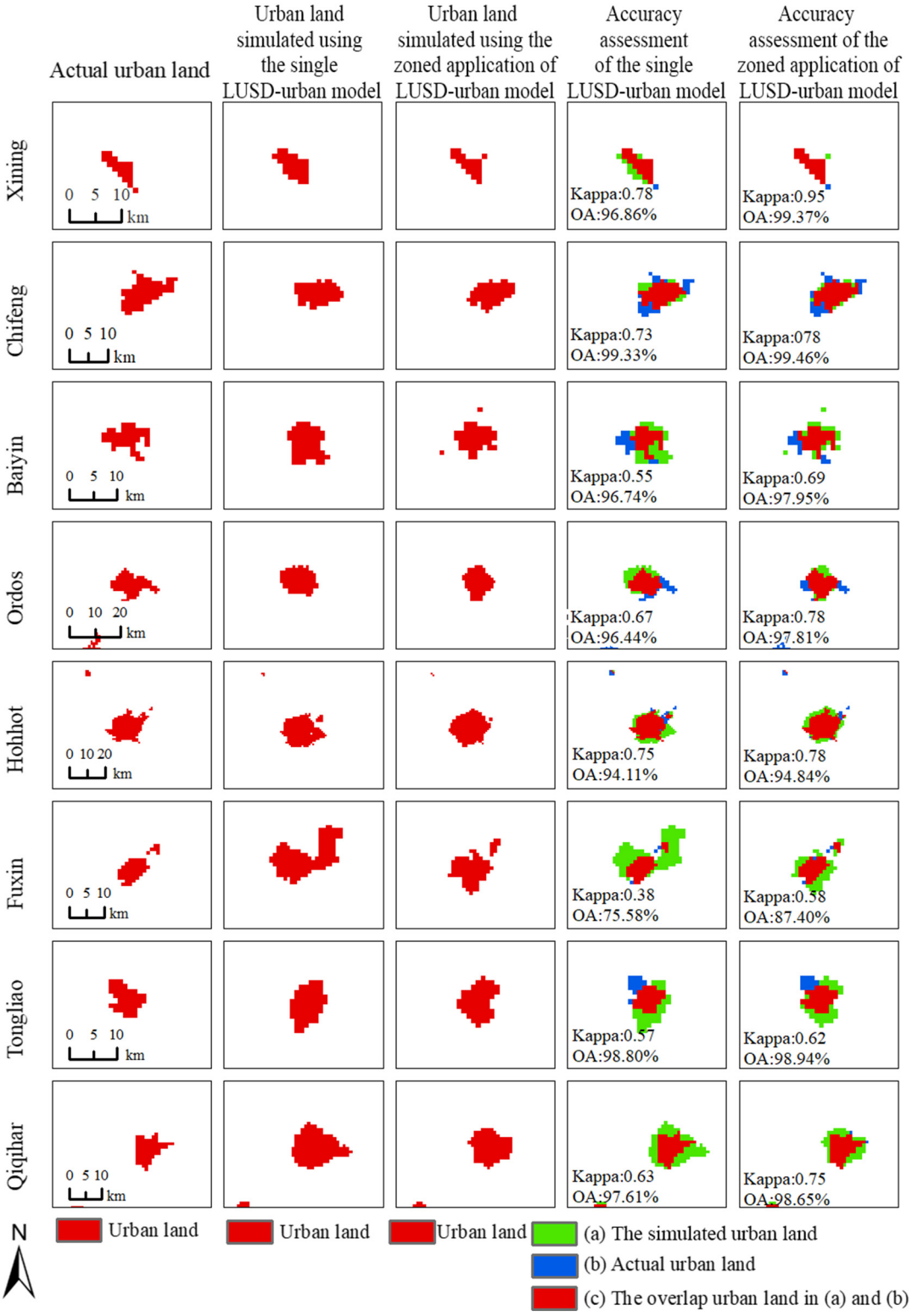

Fig. 8. The comparison of accuracy between the single LUSD-urban model and the zoned LUSD-urban model. *The eight cities with obvious difference of accuracy in 2010 were listed as examples. Please refer to Table 4 for the accuracy of the entire region in different years.

Table 5
The CCIs on urban land area.

Climate model	Scenario	Climatic region	Urban land area influenced by climate change[a] (km^2)			
			2020	2030	2040	2050
GCM	RCP2.6	Western	0.15	1.46	3.85	5.62
		Mid-western	0.12	26.34	79.17	139.07
		Mid-eastern	22.51	52.43	71.05	82.90
		Eastern	1.62	10.57	24.02	38.31
		The entire region	24.40	90.80	178.09	265.90
	RCP4.5	Western	0.15	1.97	5.63	7.63
		Mid-western	2.34	42.83	115.53	189.27
		Mid-eastern	19.88	31.15	24.66	13.02
		Eastern	1.60	10.21	22.85	36.12
		The entire region	23.97	86.16	168.67	246.04
	RCP8.5	Western	0.20	2.70	7.26	9.41
		Mid-western	2.78	48.07	128.10	205.04
		Mid-eastern	21.75	46.30	57.84	64.86
		Eastern	1.75	14.11	35.56	59.95
		The entire region	26.48	111.18	228.76	339.26
RCM	RCP2.6	Western	0.16	1.88	5.15	7.09
		Mid-western	0.32	18.95	56.52	98.70
		Mid-eastern	23.11	57.30	81.37	94.72
		Eastern	1.58	9.71	21.22	33.07
		The entire region	25.17	87.84	164.26	233.58
	RCP4.5	Western	0.14	1.43	3.77	5.52
		Mid-western	1.62	34.29	94.74	160.55
		Mid-eastern	16.97	7.67	−26.77	−68.08
		Eastern	1.51	7.85	15.17	21.72
		The entire region	20.24	51.24	86.91	119.71
	RCP8.5	Western	0.19	2.58	6.99	9.12
		Mid-western	3.03	51.14	135.47	213.88
		Mid-eastern	20.16	33.40	29.61	20.81
		Eastern	1.71	13.10	32.25	53.73
		The entire region	25.09	100.22	204.32	297.54

[a] $I = ULA_n - ULA_{ccs}$, where I denotes the urban land influenced by climate change, ULA_n denotes the urban land area under the NCCE, and ULA_{ccs} denotes the urban land area under the CCSs.

analyzing the GCM-RCPs, the urban land area potentially affected by climate change in the mid-western region will be 139.07–205.04 km^2 in 2050 (approximately 52.30%–76.93% of the urban land area potentially affected by climate change in the entire region) (Table 5, Fig. 9a). In 2050, the area of urban land potentially affected by climate change in the mid-western region will account for 8.78%–12.94% of the urban land area under the NCCE scenario, which will be 2.01–2.96 times the average level in the entire region (Fig. S5d). Under the RCM-RCPs, the urban land potentially affected by climate change in the mid-western region will be 98.70–213.88 km^2 in 2050 (approximately 42.26%–134.12% of the urban land affected by climate change in the entire region) (Table 5, Fig. 9b). In 2050, the urban land potentially affected by climate change in the mid-western region will account for 6.23%–13.5% of the urban land area under the NCCE scenario, which will be 1.63–2.77 times the average level in the entire region (Fig. S5d).

Our findings for the APTZNC are consistent with previous studies on urban expansion in drylands. For example, Magadza (2000) found that climate change will intensify water shortages in African drylands, strongly affecting urban expansion. He et al. (2015) found that the urban land affected by climate change in Beijing-Tianjin-Tangshan area will represent 20% of the total urban land in this region.

Thus, climate change will have dramatic impacts on urban expansion in drylands. Climate mitigation and adaptation measures should be awarded high priority in drylands undergoing rapid urban expansion. In terms of climate mitigation measures, it is necessary to increase urban green space, optimize urban transportation, popularize the use of clean energy and improve energy utilization efficiency (Hamin and Gurran, 2009; Shan et al., 2018). In terms of climate adaptation measures, it is necessary to improve urban morphology, increase rainwater harvesting and storage facilities, improve water resources recycling system and improve water resource utilization efficiency (Dhar and Khirfan, 2016).

5.4. Future perspectives

There are several uncertainties in this study. First, the simulation results of GCM and RCM are significantly different under the same greenhouse gas emission pathways (i.e., RCPs). Second, the water resources simulated using linear regression analysis (i.e., a function of temperature and precipitation) exhibit errors. Third, we simulated the future urban expansion primarily according to the historical urban expansion trend, ignoring that the socio-economic driving mechanism, land use policy, urban planning and the urban land suitability will change in the future with obvious influences on urban expansion (Tian et al., 2017). Therefore, the simulation results might not fully capture actual urban expansion in the future, but only possible urban expansion under different scenarios. In addition, this paper only considered the CCIs on urban land area by influencing the amount of water resources, without considering the CCIs on urban land spatial pattern. However, our results reveal the potential CCIs on urban expansion in the study area and should support climate change mitigation and adaptation efforts as well as promote sustainable development in urban landscapes.

In addition, the reasons for the regional differences in the urban expansion rate were not fully analyzed. The different urban expansion rates may be caused by two major factors: different trajectories of socioeconomic development and varying climate change trends (Table 1). The rapid urban population growth and economic development may be responsible for the fastest urban expansion in the eastern region (Xu et al., 2016). The severe water shortage and the large extent of climate change are responsible for the greatest influence of climate change on urban expansion in the mid-western region (J. Li et al., 2017).

In future research, we plan to combine the Weather Research and Forecasting (WRF) model, the Soil and Water Assessment Tool (SWAT) model and other process-based models to improve the simulation of water resources, and reveal the mechanism of the relationships between climate change and urban expansion in drylands (Blečić et al., 2014; Cao et al., 2018). We aim to further evaluate the CCIs on urban landscape spatial patterns in drylands by simulating the CCIs on land suitability and constraints (Hamin and Gurran, 2009; Dhar and Khirfan, 2016). The impacts of socio-economic drivers, land use policy, and urban planning on urban expansion as well as the reasons for regional differences will be fully analyzed (Tian et al., 2017).

6. Conclusions

We simulated the urban expansion in the APTZNC using the zoned LUSD-urban model. This method synthesizes regional differences in the influences of socio-economic development and CCIs on the urban expansion as well as the differences in urban land suitability, inheritance and neighboring effect among sub-regions. Therefore, we could effectively simulate the urban land demand and the spatial allocation of urban land. We demonstrated that our approach could reasonably simulate urban expansion in drylands under climate change.

We found that climate change will become a key factor affecting urban expansion in the APTZNC. In 2015–2050, the CCIs on regional urban expansion will continue to increase. The area of urban land affected by climate change in the entire region will increase from 20.24–26.48 km^2 (2020) to 119.71–339.26 km^2 (2050), an increase of 4.91 to 11.81 times. The CCIs on urban expansion will be the most significant in the mid-western region, where the urban land influenced by climate change would be 98.70–213.88 km^2, equivalent to 42.26%–134.12% of the urban land area influenced by climate change in the entire region.

Our findings imply that the urban expansion in the APTZNC should consider CCIs. To improve the sustainability of urban expansion, climate

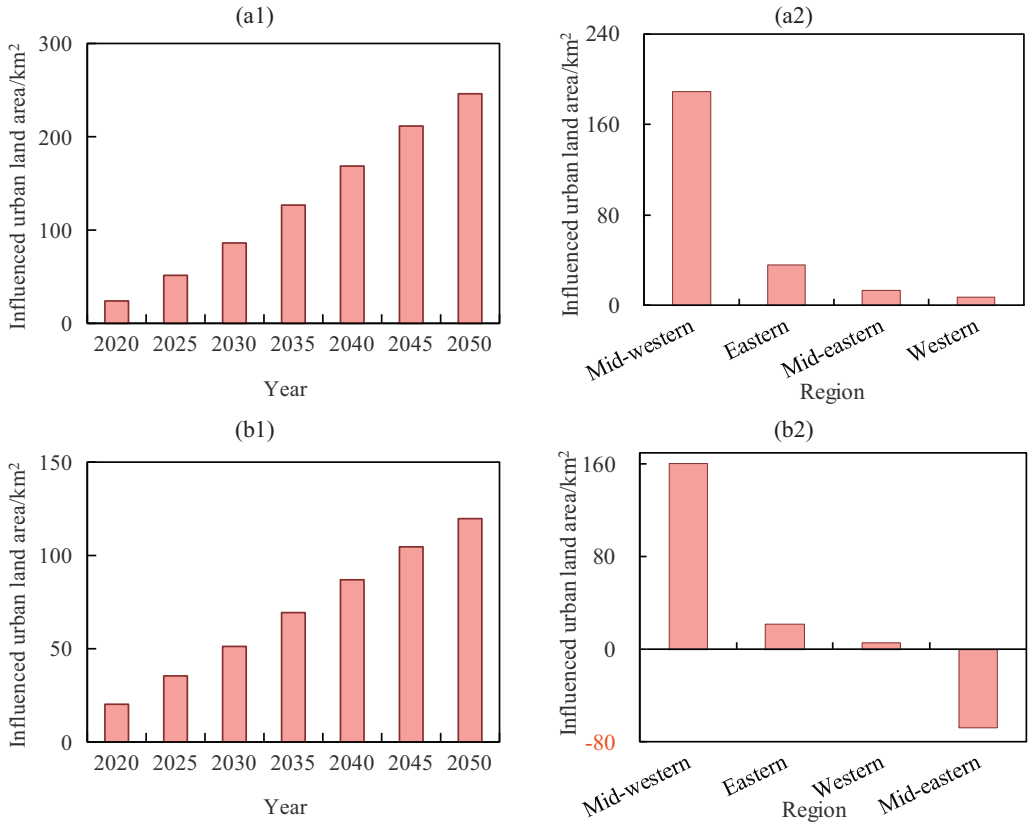

Fig. 9. The CCIs on urban land area*. (a1) The influenced urban land area in the APTZNC from 2015 to 2050 under GCM-RCP4.5. (a2) The influenced urban land area in the different regions in 2050 under GCM-RCP4.5. (b1) The influenced urban land area in the APTZNC from 2015 to 2050 under RCM-RCP4.5. (b2) The influenced urban land area in the different regions in 2050 under RCM-RCP4.5. *I=ULA_n-ULA_{ccs}, where I denotes the urban land area influenced by climate change, ULA_n denotes the urban land area under the NCCE scenario, and ULA_{ccs} denotes the urban land area under the CCSs.

mitigation and adaptation measures (such as reorganizing the composition and spatial allocation of cities, optimizing the energy structure and improving urban infrastructure) are necessary.

Acknowledgements

This work has been supported by the National Natural Science Foundation of China (Grant Nos 41871185 & 41621061). It was also supported by the Fundamental Research Funds for the Central Universities and the project from State Key Laboratory of Earth Surface Processes and Resource Ecology, China.

Appendix A. Supplementary data

Supplementary data to this article can be found online at https://doi.org/10.1016/j.scitotenv.2018.10.177.

References

Blečić, I., Cecchini, A., Falk, M., Marras, S., Pyles, D.R., Spano, D., Trunfio, G.A., 2014. Urban metabolism and climate change: a planning support system. Int. J. Appl. Earth Obs. Geoinf. 26, 447–457.

Cao, Q., Yu, D., Georgescu, M., Wu, J., Wang, W., 2018. Impacts of future urban expansion on summer climate and heat-related human health in eastern China. Environ. Int. 112, 134–146.

Cohen, J.E., 1995. Population growth and earth's human carrying capacity. Science 269 (5222), 341–346.

Deng, X., Huang, J., Lin, Y., Shi, Q., 2013. Interactions between climate, socioeconomics, and land dynamics in Qinghai province, China: a LUCD model-based numerical experiment. Advances in Meteorology. 297926, pp. 1–9.

Dhar, T.K., Khirfan, L., 2016. Climate change adaptation in the urban planning and design research: missing links and research agenda. J. Environ. Plan. Manag. 60 (4), 602–627.

Egan, P.J., Mullin, M., 2016. Recent improvement and projected worsening of weather in the United States. Nature 532 (7599), 357–360.

Giorgi, F., Coppola, E., Solmon, F., Mariotti, L., Sylla, M.B., Bi, X., Elguindi, N., Diro, G.T., Nair, V., Giuliani, G., Turuncoglu, U.U., Cozzini, S., Güttler, I., O'Brien, T.A., Tawfik, A.B., Shalaby, A., Zakey, A.S., Steiner, A.L., Stordal, F., Sloan, L.C., Brankovic, C., 2012. RegCM4: model description and preliminary tests over multiple CORDEX domains. Clim. Res. 52, 7–29.

Hamin, E.M., Gurran, N., 2009. Urban form and climate change: balancing adaptation and mitigation in the U.S. and Australia. Habitat Int. 33 (3), 238–245.

Hao, R., Yu, D., Wu, J., 2017. Relationship between paired ecosystem services in the grassland and agro-pastoral transitional zone of China using the constraint line method. Agric. Ecosyst. Environ. 240, 171–181.

He, C.Y., Shi, P.J., Chen, J., Li, X.B., Pan, Y.Z., Li, J., Li, Y.C., Li, J.G., 2005. Developing land use scenario dynamics model by the integration of system dynamics model and cellular automata model. Sci. China Ser. D Earth Sci. 48 (11), 1979–1989.

He, C.Y., Okada, N., Zhang, Q.F., Shi, P.J., Li, J.G., 2008. Modelling dynamic urban expansion processes incorporating a potential model with cellular automata. Landsc. Urban Plan. 86 (1), 79–91.

He, C., Liu, Z., Tian, J., Ma, Q., 2014. Urban expansion dynamics and natural habitat loss in China: a multiscale landscape perspective. Glob. Chang. Biol. 20 (9), 2886–2902.

He, C.Y., Zhao, Y.Y., Huang, Q.X., Zhang, Q.F., Zhang, D., 2015. Alternative future analysis for assessing the potential impact of climate change on urban landscape dynamics. Sci. Total Environ. 532, 48–60.

He, C., Li, J., Zhang, X., Liu, Z., Zhang, D., 2017. Will rapid urban expansion in the drylands of northern China continue: a scenario analysis based on the Land Use Scenario Dynamics-urban model and the Shared Socioeconomic Pathways. J. Clean. Prod. 165, 57–69.

Huang, Q., He, C., Liu, Z., Shi, P., 2014. Modeling the impacts of drying trend scenarios on land systems in northern China using an integrated SD and CA model. Sci. China Earth Sci. 57 (4), 839–854.

IPCC, 2014. Climate Change 2014: Synthesis Report. Contribution of Working Groups I, II and III to the Fifth Assessment Report of the Intergovernmental Panel on Climate Change. Cambridge University Press, Cambridge.

IPCC (Intergovernmental Panel on Climate Change), 2013. Climate Change 2013: The Physical Science Basis. IPCC WGI Fifth Assessment Report, Geneva.

Jiang, Q., Deng, X., Ke, X., Zhao, C., Zhang, W., 2014. Prediction and simulation of urban area expansion in Pearl River Delta Region under the RCPs climate scenarios. J. Appl. Ecol. 25 (12), 3627–3636.

Li, J., Liu, Z., He, C., Tu, W., Sun, Z., 2016. Are the drylands in northern China sustainable? A perspective from ecological footprint dynamics from 1990 to 2010. Sci. Total Environ. 553 (C), 223–231.

Li, X., Yu, L., Sohl, T., Clinton, N., Li, W., Zhu, Z., Liu, X., Gong, P., 2016. A cellular automata downscaling based 1 km global land use datasets (2010−2100). Sci. Bull. 61 (21), 1651–1661.
Li, J., Liu, Z., He, C., Yue, H., Gou, S., 2017. Water shortages raised a legitimate concern over the sustainable development of the drylands of northern China: evidence from the water stress index. Sci. Total Environ. 590-591, 739–750.
Li, S., Juhasz-Horvath, L., Pedde, S., Pinter, L., Rounsevell, M.D.A., Harrison, P.A., 2017. Integrated modelling of urban spatial development under uncertain climate futures: a case study in Hungary. Environ. Model. Softw. 96, 251–264.
Liu, J., Kuang, W., Zhang, Z., Xu, X., Qin, Y., Ning, J., Zhou, W., Zhang, S., Li, R., Yan, C., 2014. Spatiotemporal characteristics, patterns, and causes of land-use changes in China since the late 1980s. J. Geogr. Sci. 24 (2), 195–210.
Liu, Z., He, C., Wu, J., 2016. General spatiotemporal patterns of urbanization: an examination of 16 World cities. Sustainability 8 (1), 41.
Liu, Z., Verburg, P.H., Wu, J., He, C., 2017. Understanding land system change through scenario-based simulations: a case study from the drylands in northern China. Environ. Manag. 59 (3), 440–454.
Liu, X., Liang, X., Li, X., Xu, X., Ou, J., Chen, Y., Li, S., Wang, S., Pei, F., 2017. A future land use simulation model (FLUS) for simulating multiple land use scenarios by coupling human and natural effects. Landsc. Urban Plan. 168, 94–116.
Liu, Y., Li, J., Qin, K., Chen, D., 2018. Simulating and analyzing the change of land use and ecosystem services in Guanzhong plain based on scenarios. J. Shaanxi Normal Univ. Nat. Sci. Ed. 46 (2), 95–103.
Long, T.R., Jiang, W.C., He, Q., 2004. Water resources carrying capacity: new perspectives based on eco-economic analysis and sustainable development. J. Hydraul. Eng. 1, 38–45.
Magadza, C.H.D., 2000. Climate change impacts and human settlements in Africa: prospects for adaptation. Environ. Monit. Assess. 61, 193–205.
McDonald, R.I., Green, P., Balk, D., Fekete, B.M., Revenga, C., Todd, M., Montgomery, M., 2011. Urban growth, climate change, and freshwater availability. Proc. Natl. Acad. Sci. U. S. A. 108 (15), 6312–6317.
MEA. (Millennium Ecosystem Assessment), 2005. Ecosystems and Human Well-being. Synthesis. Island Press, Washington DC, p. vol. 42.
Moss, R.H., Edmonds, J.A., Hibbard, K.A., Manning, M.R., Rose, S.K., van Vuuren, D.P., Carter, T.R., Emori, S., Kainuma, M., Kram, T., Meehl, G.A., Mitchell, J.F., Nakicenovic, N., Riahi, K., Smith, S.J., Stouffer, R.J., Thomson, A.M., Weyant, J.P., Wilbanks, T.J., 2010. The next generation of scenarios for climate change research and assessment. Nature 463 (7282), 747–756.
National Bureau of Statistics of China (NBSC), 2016. China Statistical Yearbook 2016. China Statistics Press, Beijing.
Pei, F., Li, X., Liu, X., Wang, S., He, Z., 2013. Assessing the differences in net primary productivity between pre-and post-urban land development in China. Agric. For. Meteorol. 171, 174–186.
Pravalie, R., 2016. Drylands extent and environmental issues. A global approach. Earth Sci. Rev. 161, 259–278.
Reynolds, J.F., Stafford Smith, D.M., Lambin, E.F., Turner, B.L., Mortimore, M., Batterbury, S.P.J., Downing, T.E., Dowlatabadi, H., Fernandez, R.J., Herrick, J.E., Huber-Sannwald, E., Jiang, H., Leemans, R., Lynam, T., Maestre, F.T., Ayarza, M., Walker, B., 2007. Global desertification: building a science for dryland development. Science 316 (5826), 847–851.
Schimel, D.S., 2010. Drylands in the earth system. Science 327 (5964), 418–419.
Shan, Y., Guan, D., Hubacek, K., Zheng, B., Davis, S.J., Jia, L., Liu, J., Liu, Z., Fromer, N., Mi, Z., Meng, J., Deng, X., Li, Y., Lin, J., Schroeder, H., Weisz, H., Schellnhuber, H.J., 2018. City-level climate change mitigation in China. Sci. Adv. 4, eaaq0390.
Shen, Q., Chen, Q., Tang, B.-s., Yeung, S., Hu, Y., Cheung, G., 2009. A system dynamics model for the sustainable land use planning and development. Habitat Int. 33 (1), 15–25.
Shi, P., Li, X., Song, B., 2009. Land Use Pattern and Optimization Simulation in Farming-pastoral Zone of Northen China. Science Press, Beijing (in Chinese).
Shi, P., Sun, S., Wang, M., Li, N., Wang, J.A., Jin, Y., Gu, X., Yin, W., 2014. Climate change regionalization in China (1961–2010). Sci. China Earth Sci. 57 (11), 2676–2689.
Tian, L., Li, Y., Yan, Y., Wang, B., 2017. Measuring urban sprawl and exploring the role planning plays: a shanghai case study. Land Use Policy 67, 426–435.
UN (United Nations), 2014. World urbanization prospects, the 2014 revision. http://esa.un.org/unpd/wup/.
UNDP-DDC (United Nations Development Programme-Drylands Development Centre), 2007. Working with people to fight poverty in the dry areas of the world: UNDP drylands development centre activity report 2002–2006. http://web.undp.org/drylands.
UNDP-DDC (United Nations Development Programme-Drylands Development Centre), 2014. Integrated drylands development programme. http://web.undp.org/drylands/iddp.html.
van Vuuren, D.P., Edmonds, J., Kainuma, M., Riahi, K., Thomson, A., Hibbard, K., Hurtt, G.C., Kram, T., Krey, V., Lamarque, J.-F., Masui, T., Meinshausen, M., Nakicenovic, N., Smith, S.J., Rose, S.K., 2011. The representative concentration pathways: an overview. Clim. Chang. 109 (1), 5.
Verburg, P.H., Tabeau, A., Hatna, E., 2013. Assessing spatial uncertainties of land allocation using a scenario approach and sensitivity analysis: a study for land use in Europe. J. Environ. Manag. 127, S132–S144 (Suppl).
Wang, J., Xu, X., Liu, P., 1999. Land use and land carrying capacity in ecotone between agriculture and animal husbandry in northern China. Resour. Sci. 21 (5), 19–24 (in Chinese).
Wu, J., 2013. Landscape sustainability science: ecosystem services and human well-being in changing landscapes. Landsc. Ecol. 28, 999–1023.
Wu, J., 2014. Urban ecology and sustainability: the state-of-the-science and future directions. Landsc. Urban Plan. 125, 209–221.
Xie, G., Zhou, H., Zhen, L., Xiao, Y., 2005. Carrying capacity of water resources for China's development. Res. Sci. 27, 2–7.
Xu, M., He, C., Liu, Z., Dou, Y., 2016. How did urban land expand in China between 1992 and 2015? A multi-scale landscape analysis. PLoS One 11 (5), e0154839.